Volume 18
Number 8
August 1979

Inorganic Chemistry

Contribution from the Department of Chemistry,
King's College, Strand, London WC2R 2LS, England

Complexes of the Platinum Metals. 17.[1] Molecular Dynamics of the Species $[M(O_2CR)_2(CO)(PPh_3)_2]$ (M = Ru, R = Me, CF_3, C_2F_5, C_6F_5; M = Os, R = Me, CF_3)

CLIFFORD J. CRESWELL,*[2] ALAN DOBSON, DAVID S. MOORE, and STEPHEN D. ROBINSON*

Received December 15, 1978

Intramolecular monodentate–bidentate carboxylate ligand exchange in the complexes $[M(O_2CR)_2(CO)(PPh_3)_2]$ (M = Ru, R = Me, CF_3, C_2F_5, C_6F_5; M = Os, R = Me, CF_3) has been studied by variable-temperature ^{31}P and ^1H or ^{19}F NMR. Kinetic data establish the participation of two mechanisms—a fast process involving cleavage of Ru–O bonds trans to phosphorus and a slower one involving rupture of the Ru–O bond trans to carbonyl. In the presence of methanol or similar oxygen donors (L) species of the form $[Ru(O_2CR)_2(CO)L(PPh_3)_2]$ and/or $[Ru(O_2CR)(CO)L(PPh_3)_2][O_2CR]$ also participate in the rate processes. Values for thermodynamic parameters of activation are recorded.

Introduction

As part of a study of platinum metal carboxylato complexes, we have previously described new ruthenium(II) and osmium(II) derivatives $[M(O_2CR)_2(CO)(PPh_3)_2]$ (R = alkyl, aryl, perfluoroalkyl, perfluoroaryl)[3,4] and have reported on their ability to catalyze the dehydrogenation of primary and secondary alcohols.[5] We have also established that these complexes possess stereochemistry I and have detected, by

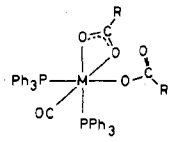

(I)

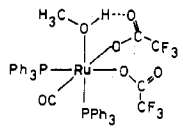

(II)

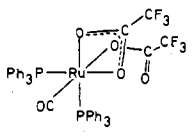

(III)

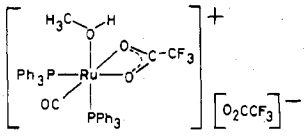

(IV)

variable-temperature NMR spectroscopy, the rapid intramolecular exchange of the mono- and bidentate carboxylate ligands.[3,4] In view of our interest in the alcohol dehydrogenation catalysis[5] and the general paucity of kinetic and mechanistic data on "fluxional" carboxylato complexes,[6] we have conducted, and now report, a detailed study of these complexes and their methanol solvates (stereochemistry II) by variable-temperature NMR spectroscopy.

Experimental Section

Complexes were prepared as previously described.[3,4] Spectra were obtained by using a Bruker HFX-90 spectrometer, equipped with a Nicolet 1080 data system for Fourier-transform pulsed NMR. The ^{31}P (^1H broad band decoupled) and ^1H NMR data were obtained at 36.43 and 90.00 MHz, respectively, with the spectrometer operating in Fourier-transform mode. A pulse width of 10 μs, corresponding to a flip angle of 25°, was employed and 1000–4000 pulses were generally accumulated. The ^{19}F data were obtained with the spectrometer operating in continuous-wave mode at a frequency of 84.66 MHz. Generally 500 scans were accumulated. All spectra were obtained by using a deuterium lock. The rf power was always maintained below the level at which saturation effects occurred. A variable-temperature probe fitted with a Bruker controller and calibrated with a Varian standard methyl alcohol sample was used to maintain selected temperatures to ±0.5 °C. The ^1H chemical shifts were recorded relative to an internal tetramethylsilane standard and are reported in ppm with positive values indicating resonances at low field relative to Me_4Si. The ^{31}P chemical shifts were recorded relative to an external standard of 85% H_3PO_4 and are reported in ppm with a positive value indicating a resonance at low field relative to H_3PO_4. The ^{19}F chemical shifts were recorded relative to an internal trichlorofluoromethane standard and are reported in ppm with a positive value indicating a resonance at high field relative to $CFCl_3$. Unless otherwise indicated, samples were examined by using deuteriochloroform as solvent. The calculations were performed by means of a computer simulation procedure with a Nicolet 1080 computer and a two-site exchange program[7] based on the Gutowsky and Holm equations[8-10] for chemical exchange. This two-site exchange program, which allows for coupling between two nuclei each with a spin of $^1/_2$ to give an AB spectrum in the slow-exchange limit, iteratively fits the chemical shifts ν_1 and ν_2, the line width parameter $\Delta\nu_{1/2}$ (line width at half-height in absence of exchange), the coupling constant J, and the average rate constant, k, for the forward and reverse directions, to an NMR line shape broadened by chemical exchange.

The temperature dependence of the chemical shifts was taken into account by obtaining values for temperatures below coalescence by iterative evaluation or by direct measurement at temperatures below the region where exchange broadening is observed and by using extrapolation on a plot of shifts vs. temperature to estimate values in the region above the coalescence temperature. However, values for $\Delta\nu_{1/2}$ determined at high temperature (rapid exchange) and low temperature (very slow exchange) where the line shape is not affected by the exchange process were found to be constant within experimental error. Therefore, a constant value of $\Delta\nu_{1/2}$ was maintained in the calculations throughout the temperature range of interest. Small uncertainties in the values of $\Delta\nu_{1/2}$ and the chemical shifts in the ^{31}P NMR spectra had very little influence on the calculated values of the rate constants, k, because of the substantial differences in the chemical shifts of the two sites undergoing exchange.

The rate constant, k, was iteratively evaluated from exchange-broadened spectra at each of ca. ten different temperatures.

0020-1669/79/1318-2055$01.00/0

Table VII. NMR Data

complex	nuclei	T_D/K[a]	ν_1/ppm	ν_2/ppm	J/Hz	$\Delta\nu_{1/2}$/Hz	T_c/K[b]
$[Ru(O_2CMe)_2(CO)(PPh_3)_2]$	^{31}P	211	48.72	45.40	24.4	5.2	243 ± 2
	^{1}H	230	1.44	1.14		2.4	270 ± 1
$[Ru(O_2CCF_3)_2(CO)(PPh_3)_2]$	^{31}P	220	44.03	40.30	29.9	3.9	266 ± 1
	^{19}F	260	76.72	76.47		2.3	298 ± 1
$[Ru(O_2CC_2F_5)_2(CO)(PPh_3)_2]$	^{31}P	213	43.63	39.38	29.7	4.4	260 ± 1
$[Ru(O_2CC_6F_5)_2(CO)(PPh_3)_2]$	^{31}P	205	50.64	44.91	28.0	4.5	232 ± 1
	^{31}P[c]	205	(44.91)	40.61	29.0		
$[Os(O_2CMe)_2(CO)(PPh_3)_2]$	^{31}P	245	6.56	4.14	7.8	4.7	294 ± 1
	^{1}H	270	1.57	1.16		2.5	294 ± 1
$[Os(O_2CCF_3)_2(CO)(PPh_3)_2]$	^{31}P	270	−3.02	−4.08	11.8	3.8	294 ± 1
	^{19}F	278	75.44	75.22		2.35	311 ± 1

[a] T_D is the lowest temperature recorded, used to measure the chemical shifts ν_1 and ν_2. [b] T_c is the coalescence temperature. [c] Data refer to extra resonance (see text).

Table VIII. Activation Data[a]

complex	NMR data source	E_a/kJ mol^{-1}	$\Delta H^{\ddagger}$/kJ mol^{-1}	$\Delta S^{\ddagger}$/J K^{-1} mol^{-1}	$\Delta G^{\ddagger}$/kJ mol^{-1}	T_c/K
$[Ru(O_2CMe)_2(CO)(PPh_3)_2]$	^{31}P	45.9 ± 2.5	44.0 ± 2.5	−8 ± 8	46.0 ± 2.0	243 ± 2
	^{1}H	53.8 ± 2.0	51.5 ± 2.0	−15 ± 6	55.6 ± 2.0	270 ± 1
$[Ru(O_2CCF_3)_2(CO)(PPh_3)_2]$	^{31}P	54.7 ± 1.5	52.6 ± 1.5	8.6 ± 6	50.4 ± 1.5	266 ± 1
	^{19}F	58.0 ± 1.5	55.5 ± 1.5	−22 ± 6	62.0 ± 2.0	298 ± 1
$[Ru(O_2CC_2F_5)_2(CO)(PPh_3)_2]$	^{31}P	56.0 ± 1.7	54.0 ± 1.7	12.5 ± 7	50.75 ± 1.7	260 ± 1
$[Ru(O_2CC_6F_5)_2(CO)(PPh_3)_2]$	^{31}P	51.5 ± 1.0	49.6 ± 1.0	18.6 ± 4	45.2 ± 1.0	232 ± 1
$[Os(O_2CMe)_2(CO)(PPh_3)_2]$	^{31}P	60.9 ± 1.5	58.6 ± 1.5	7.5 ± 5	56.5 ± 1.5	294 ± 1
	^{1}H	65.5 ± 2.5	63.0 ± 2.5	11.8 ± 8	59.5 ± 2.5	294 ± 1
$[Os(O_2CCF_3)_2(CO)(PPh_3)_2]$	^{31}P	64.6 ± 3.5	62.2 ± 3.5	0 ± 12	61.9 ± 3.5	294 ± 1
	^{19}F	71.8 ± 3.9	69.3 ± 3.9	6.5 ± 13	67.3 ± 3.9	311 ± 1

[a] All data refer to coalescence temperature (T_c).

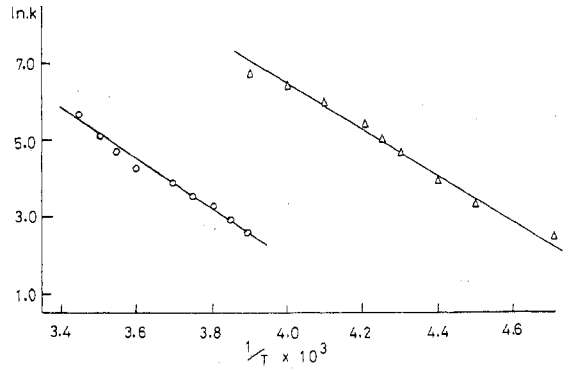

Figure 1. Arrhenius plots for $[Ru(O_2CMe)_2(CO)(PPh_3)_2]$: (△) data obtained from ^{31}P NMR spectra; (○) data obtained from ^{1}H NMR spectra.

Thermodynamic activation parameters were calculated according to the Eyring theory.[11,12] The $\Delta H^{\ddagger}$ and $\Delta S^{\ddagger}$ values were obtained from a least-squares treatment of the corresponding rate data. The $\Delta G^{\ddagger}$ values were calculated from the equation $\Delta G^{\ddagger} = \Delta H^{\ddagger} - T\Delta S^{\ddagger}$ where T is the coalescence temperature (T_c). Estimated maximum errors, which allow for uncertainties in chemical shifts and $\Delta\nu_{1/2}$ values, are reported with the activation data in Tables I–VI and VIII.

Results and Discussion

Experimental data collected for individual complexes are presented in Tables I–VI (supplementary material). The significant NMR and activation data are correlated in Tables VII and VIII and are collectively evaluated after the discussion of individual compounds.

$[Ru(O_2CMe)_2(CO)(PPh_3)_2]$. The spectra recorded for this complex display a ^{31}P NMR singlet which decoalesces at low temperature (ca. 243 K) to afford an AB pattern and an ^{1}H(methyl) singlet which similarly decoalesces (ca. 270 K) to two peaks of equal intensity.[13] These data confirm the established stereochemistry (I, M = Ru, R = Me) and the rapid intramolecular exchange of the monodentate and bidentate acetate ligands. Arrhenius plots (Figure 1) derived

Scheme I. Mechanism for Interchange of Phosphine Ligands but Not Acetate Ligands in $[Ru(O_2CMe)_2(CO)(PPh_3)_2]$

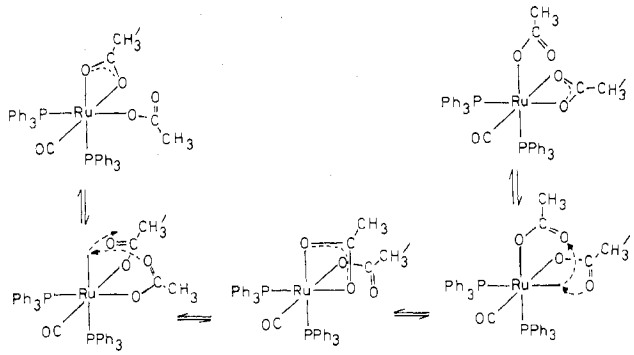

Scheme II. Mechanism for Interchange of Phosphine Ligands and of Acetate Ligands in $[Ru(O_2CMe)_2(CO)(PPh_3)_2]$

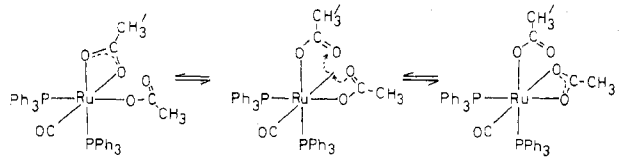

from the experimental (^{31}P and ^{1}H NMR) data (Table I) clearly establish that two distinct rate processes with significantly different activation parameters govern the equilibration of the triphenylphosphine (^{31}P) ligands and interchange of the acetate (^{1}H) ligands. For an explanation of these results two mechanisms involving partial or complete interchange of the mono- and bidentate acetate ligands are proposed. Scheme I, involving cleavage of the Ru–O bonds trans to phosphine but not carbonyl, renders the phosphine (^{31}P nuclei) equivalent on the NMR time scale and exchanges the roles of the mono- and bidentate acetate ligands. However, the carboxylate groups are not fully equilibrated since the coordination site trans to the carbonyl ligand is retained throughout by one

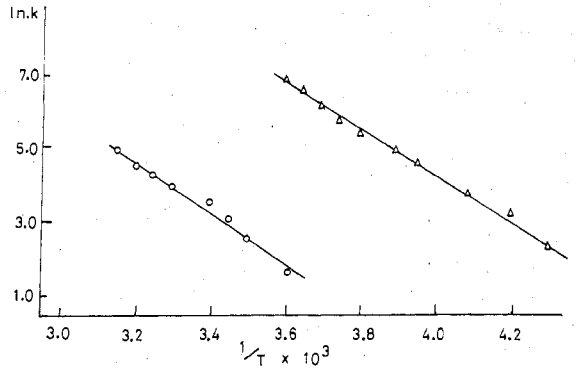

Figure 2. Arrhenius plots for $[Ru(O_2CCF_3)_2(CO)(PPh_3)_2]$: (Δ) data obtained from ^{31}P NMR spectra; (O) data obtained from ^{19}F NMR spectra.

particular acetate ligand.[14] Equilibration of the phosphine ligands could occur by a twist mechanism. However such mechanisms have been eliminated in the case of phosphine interchange in the complexes *cis*-$[Ru(S_2PMe_2)_2(PR_3)_2]$[15] and, given the greater lability of Ru–O bonds relative to Ru–S bonds, are therefore considered improbable in the present system. Scheme II, involving cleavage of the Ru–O bond trans to carbonyl, equilibrates the acetate ligands as well as the phosphine ligands. According to these schemes increasing sample temperature accelerates the ligand interchange processes leading first to equilibration of the phosphine ligands (^{31}P nuclei), by virtue of the monodentate–bidentate acetate exchange (Scheme I), and subsequently to complete equilibration of the acetate ligands as a consequence of the labilization of the remaining Ru–O linkage (trans to CO) (Scheme II). Thus at the higher temperatures a combination of Schemes I and II leads to complete equilibration of the phosphine ligands and of the acetate ligands. Other workers have shown[15] that in the ruthenium(II) complexes $[Ru(S_2PMe_2)_2LL']$ (L and L′ = phosphine and/or carbonyl) the Ru–S bonds trans to phosphine are more labile than those trans to carbonyl. This observation is also in accord with the known trans-labilizing capacities of phosphine and carbonyl ligands.[16,17] Therefore, the mechanisms presented in Schemes I and II are fully consistent with the NMR data and with the available chemical evidence. Activation data for the processes illustrated in Schemes I and II are summarized in Table VIII. Alternative mechanisms involving dissociation of triphenylphosphine ligands, solvent participation, or formation of binuclear intermediates were examined and eliminated. Thus addition of free phosphine, change of solvent ($CDCl_3 \rightarrow C_6D_5CD_3$), or dilution of sample concentration (×4) produced no detectable change in the variable-temperature NMR spectra. More radical changes of solvent were precluded by solubility problems. Other workers[15] examining the interchange of monodentate and bidentate (dimethylphosphino)dithioate ligands in the solvated complexes $[Ru(S_2PMe_2)_2(PR_3)_2(Sol^v)]$ (PR_3 = PPh_3, etc.) similarly found no evidence of phosphine dissociation or involvement of binuclear intermediates and attributed the observed solvent dependence to the initial solvation process rather than the actual monodentate–bidentate ligand interchange step.

$[Ru(O_2CCF_3)_2(CO)(PPh_3)_2]$. The ^{31}P and ^{19}F NMR data recorded for this complex are qualitatively similar to the ^{31}P and ^1H data obtained for the corresponding acetato derivative and are therefore amenable to a similar interpretation. Detailed experimental data are recorded in Table II and were employed to obtain the Arrhenius plots shown in Figure 2. The relevant thermodynamic data are summarized in Table VIII.

$[Ru(O_2CC_2F_5)_2(CO)(PPh_3)_2]$. The ^{31}P NMR spectra (Tables III and VII) and derived thermodynamic data (Tables III and VIII) obtained for this complex agree closely with those recorded for the corresponding trifluoroacetato derivative. No attempt was made to analyze the ^{19}F spectrum which consisted of a broad envelope at ca. 300 K and decoalesced to a complex pattern at lower temperatures.

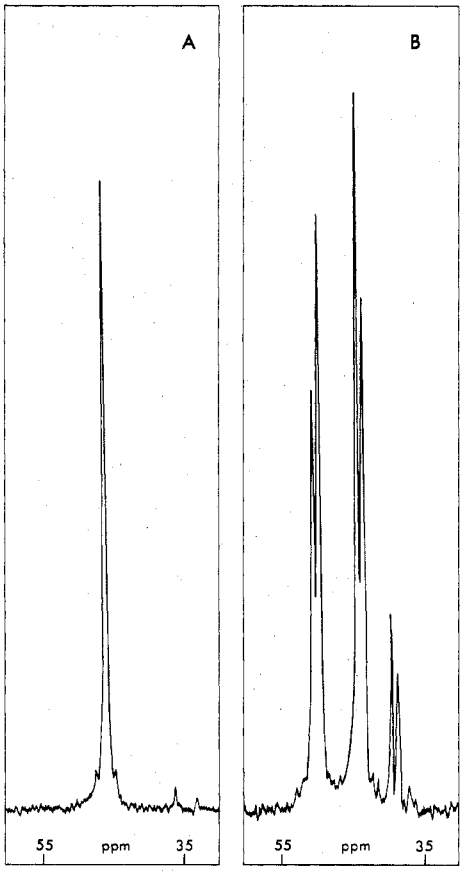

Figure 3. ^{31}P NMR spectra of $[Ru(O_2CC_6F_5)_2(CO)(PPh_3)_2]$: (A) recorded at 295 K, (B) recorded at 205 K.

$[Ru(O_2CC_6F_5)_2(CO)(PPh_3)_2]$. The ^{31}P NMR data obtained for the pentafluorobenzoate (Tables IV and VII) give values for the thermodynamic parameters of activation (Tables IV and VIII) which differ significantly from those recorded for the corresponding trifluoroacetato and pentafluoropropionato complexes. However, the data for $[Ru(O_2CC_6F_5)_2(CO)(PPh_3)_2]$ must be interpreted with due caution since all ^{31}P NMR spectra obtained for this complex displayed an extra resonance pattern at low temperatures. This additional resonance, which appeared to be an AB pattern half submerged under the main signal (Figure 3), collapsed (240 K) and merged into the latter on warming the sample to ca. 290 K. The presence of this extra signal seriously interfered with the computer line-shape analysis and thereby reduced the credibility of the resultant thermodynamic data. The origin of the extra signal was not ascertained. However, its absorption into the main signal at high temperatures clearly indicates that the species involved is in labile equilibrium with the major component of the mixture. Addition of small amounts of various donor solvents (MeOH, Et_2O, or H_2O) did not materially alter the shape or position of the extra signal. We therefore conclude that solvation processes (vide infra) are not responsible for the appearance of the "extra" signal. The most plausible explanation, in our view, is one involving a small population of a second conformer at low temperatures, in which an alternative packing of the bulky pentafluorophenyl moieties in the coordination sphere prevails. It is conceivable that the second conformer may involve chelation of the bidentate pentafluorobenzoate ligand through an ortho fluorine atom

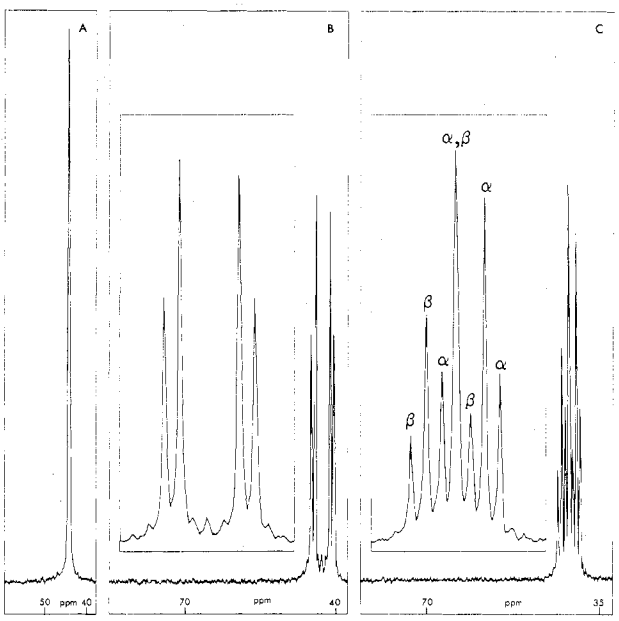

Figure 4. ^{31}P NMR spectra of $[Ru(O_2CCF_3)_2(CO)(PPh_3)_2]$: (A) recorded at 295 K, (B) recorded at 220 K (expanded signal inset), (C) recorded at 220 K in the presence of ca. 1.0 mol of methanol/mol of complex (expanded signal inset). Note: The AB pattern arising from $[Ru(O_2CCF_3)_2(CO)(PPh_3)_2]$ displays a methanol concentration dependent chemical shift owing to the formation of a very labile H-bonded intermediate (Scheme III and text). The AB patterns arising from solvated and nonsolvated complexes are labeled α and β, respectively.

rather than the second O-donor site. However, we have been unable to obtain supporting evidence for this hypothesis.

$[Os(O_2CMe)_2(CO)(PPh_3)_2]$. The ^{31}P and ^1H NMR data recorded for this complex are qualitatively similar to those obtained for the corresponding ruthenium compound. Detailed experimental data are recorded in Tables V and VII, and the relevant activation data are summarized in Table VIII.

$[Os(O_2CCF_3)_2(CO)(PPh_3)_2]$. The ^{31}P and ^{19}F NMR data for this complex are recorded in Tables VI and VII and are qualitatively similar to those obtained for the analogous ruthenium compound. The relevant activation data are summarized in Table VIII.

$[Ru(O_2CCF_3)_2(CO)(PPh_3)_2]$/MeOH. In view of the role of alcohol solvates as intermediates in the catalytic dehydrogenation of primary and secondary alcohols by the complexes $[M(O_2CR_F)_2(CO)(PPh_3)_2]$ (M = Ru or Os; $R_F = CF_3$, C_2F_5, etc.)[5] and their possible relevance to the mechanism of the monodentate–bidentate carboxylate ligand interchange process, the variable-temperature NMR spectra of $[Ru(O_2CCF_3)_2(CO)(PPh_3)_2]$ in the presence of small amounts of methanol have been examined.

Addition of small portions of methanol (ca. 0.2–2.0 mol/mol of complex) to an NMR sample of the complex $[Ru(O_2CCF_3)_2(CO)(PPh_3)_2]$ in deuteriochloroform at low temperature (ca. 220 K) led to the progressive growth of a new ^{31}P NMR AB pattern at the expense of the original AB pattern (Figure 4). The relative positions of the two AB patterns are also dependent upon the concentration of added methanol. On warming of the sample to ca. 220–300 K, the two signals broaden and subsequently merge into a single sharp resonance. We attribute the second AB pattern to the presence in solution of the methanol solvated complex, $[Ru(O_2CCF_3)_2(CO)(MeOH)(PPh_3)_2]$, which has previously been isolated from the reaction of $[Ru(O_2CCF_3)_2(CO)(PPh_3)_2]$ with methanol and has been shown by X-ray diffraction methods to possess structure and stereochemistry II.[18] Examination of the relative intensities of the two AB patterns establishes that the solvated

Scheme III. Mechanism for Solvation of $[Ru(O_2CCF_3)_2(CO)(PPh_3)_2]$ by Methanol[a]

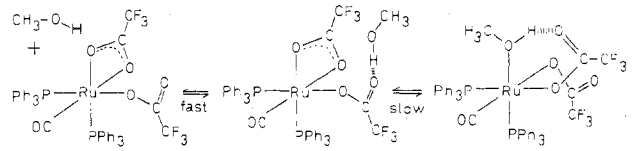

[a] In this scheme and in Scheme IV the methanol is shown H bonding to one particular carboxylate; however, both carboxylates are assumed to participate in the labile H-bonding equilibria.

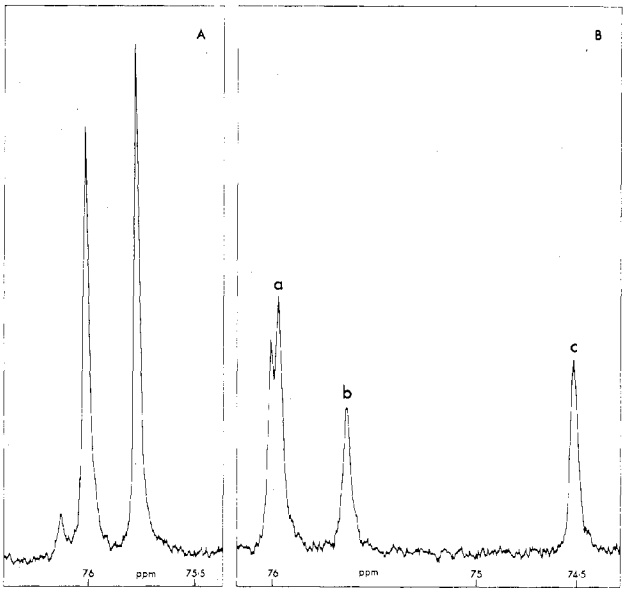

Figure 5. ^{19}F NMR spectrum of $[Ru(O_2CCF_3)_2(CO)(PPh_3)_2]$ recorded at 220 K: (A) in the absence of added methanol, (B) in the presence of ca. 0.5 mol of methanol/mol of complex. Note: The pattern arising from $[Ru(O_2CCF_3)_2(CO)(PPh_3)_2]$ displays a methanol concentration dependent chemical shift owing to the formation of a very labile H-bonded intermediate (Scheme III and text).

complex becomes the dominant species present in solution when the methanol/complex ratio exceeds ca. 2/1. At high methanol concentrations a third AB pattern of very low intensity can be detected. We tentatively attribute this to a low concentration of the salt $[Ru(O_2CCF_3)(CO)(MeOH)(PPh_3)_2][O_2CCF_3]$ (stereochemistry IV). Conductivity measurements on methanol solutions of $[Ru(O_2CCF_3)_2(CO)(PPh_3)_2]$ are compatible with the presence of a salt in very low concentrations. The observed shift in the position of the original AB pattern on addition of methanol is attributed to the occurrence of a dynamic equilibrium process involving a very labile hydrogen-bonded intermediate (Scheme III).

Addition of methanol produces a parallel sequence of changes in the ^{19}F NMR spectrum. The singlet observed at high temperatures decoalesces to a pair of equal lines on cooling in the absence of methanol but generates a more complex pattern containing three broad resonances (Figure 5) when examined at low temperature in the presence of methanol. One component (a) of this pattern has an integrated intensity equal, within experimental error, to the sum of the other two (b + c) and under favorable circumstances can be resolved into two separate resonances. Given that the structures of the nonsolvated and methanol solvated complex are I and II, respectively, it follows that the major component (a) must be attributed to monodentate trifluoroacetate ligands trans to triphenylphosphine since they represent 50% of the total trifluoroacetate present. The remaining pair of components (b) and (c) which broaden and coalesce together

Scheme IV. Mechanism for Solvation and Ligand Interchange in $[Ru(O_2CCF_3)_2(CO)(PPh_3)_2]$ in the Presence of Methanol

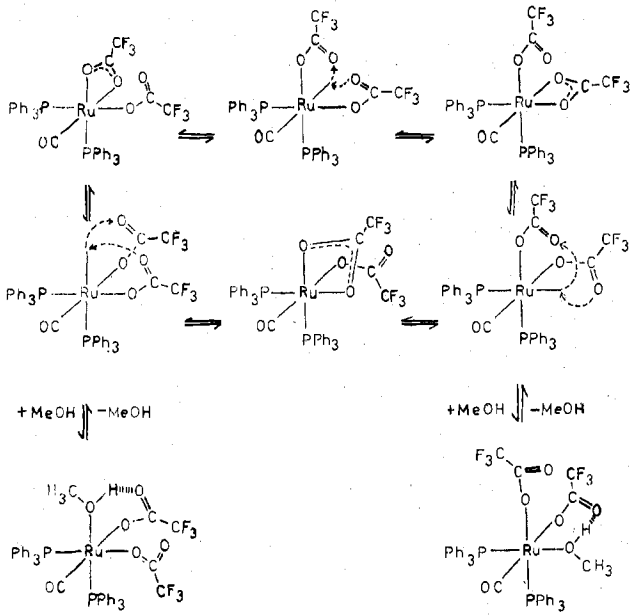

before coalescing with component (a) must be attributed to bidentate and monodentate (trans to carbonyl) trifluoroacetate ligands. Since the low-temperature ^{19}F NMR spectrum of the nonsolvated complex displays two resonances corresponding to those labeled (a) and (b) in Figure 5, it follows that component (b) must be due to the bidentate trifluoroacetate ligand and that component (c) must arise from monodentate trifluoroacetate trans to carbonyl. Changes observed in the relative intensities of the three components (a–c) as the concentration of methanol is increased confirm these assignments.

Since components (b) and (c) broaden and coalesce at much lower temperature than component (a), we conclude that only one trifluoroacetate ligand (trans to CO) competes directly with methanol for the third coordination site and that the remaining trifluoroacetate participates only by virtue of the trifluoroacetate ligand interchange process described above for the nonsolvated complex. This conclusion is in accord with our earlier observation (vide supra) that isomer III does not occur in detectable quantities in the equilibria involving the nonsolvated complex (Scheme IV). The observed methanol concentration dependence of the ^{31}P resonance positions (a and b) is further evidence for formation of the labile hydrogen-bonded intermediate noted above and illustrated in Scheme III.

Examination of the collected data in Tables VII and VIII leads to a number of general observations and permits some tentative deductions to be made.

As anticipated the activation parameters establish that the ruthenium complexes are more labile than their osmium analogues. They also indicate that for a given metal the lability of the interchange reactions increases with change of ligand in the sequence $C_6F_5CO_2 \sim CF_3CO_2 < MeCO_2 < NO_3$.[19,20] This trend is paralleled by increasing ligand coordinating power and reducing ligand size. It is therefore inconsistent with a dissociative rate-determining step where bond breaking is expected to be a dominant factor. However, it is compatible with a concerted step where metal–ligand bond making and breaking processes are of essentially similar importance and where a reduction in ligand size would be expected to facilitate a concerted mechanism involving formation of an associative intermediate. The entropies of activation have relatively small negative or, more usually, small positive values and, given the uncertainty surrounding the possible contributory factors, do not decisively support either an associative or a dissociative mechanism. However, the close agreement between the E_a, $\Delta H^{\ddagger}$, $\Delta G^{\ddagger}$, and $\Delta S^{\ddagger}$ values observed in the present work and those reported by Cole-Hamilton and Stephenson for the rapid interchange of mono- and bidentate S-donor ligands in the solvated complex $[Ru(S_2PMe_2)_2(PPh_3)_2(Sol^v)]$ in chloroform solution strongly supports our tentative conclusion that the rate-determining step in these systems is a concerted one with essentially similar contributions from bond making and breaking.

Acknowledgment. We thank Dr. D. A. Couch and Mrs. E. Summers for obtaining the NMR spectra, Johnson Matthey & Co., Ltd., for a generous loan of platinum metal salts, and the Science Research Council for grants to A.D. and D.S.M.

Registry No. $Ru(O_2CMe)_2(CO)(PPh_3)_2$, 61990-12-3; $Ru(O_2CCF_3)_2(CO)(PPh_3)_2$, 55222-16-7; $Ru(O_2CC_2F_5)_2(CO)(PPh_3)_2$, 70224-18-9; $Ru(O_2CC_6F_5)(CO)(PPh_3)_2$, 70267-72-0; $Os(O_2CMe)_2(CO)(PPh_3)_2$, 61990-13-4; $Os(O_2CCF_3)_2(CO)(PPh_3)_2$, 70224-19-0.

Supplementary Material Available: Tables I–VI giving detailed NMR data (6 pages). Ordering information is given on any current masthead page.

References and Notes

(1) Part 16: D. S. Moore and S. D. Robinson, *Inorg. Chem.*, companion paper in Notes section of this issue.
(2) Address correspondence to this author at the Department of Chemistry, Hamline University, St. Paul, Minnesota 55101.
(3) S. D. Robinson and M. F. Uttley, *J. Chem. Soc., Dalton Trans.*, 1912 (1973).
(4) A. Dobson and S. D. Robinson, *J. Chem. Soc., Dalton Trans.*, 370 (1975).
(5) A. Dobson and S. D. Robinson, *Inorg. Chem.*, **16**, 137 (1977).
(6) Studies on these systems appear to be confined to the work of Powell et al. and van Leeuwen et al. on carboxylate-bridged binuclear complexes of palladium(II) and platinum(II): J. Powell, *J. Am. Chem. Soc.*, **91**, 4311 (1969); *J. Chem. Soc. A*, 2233 (1971); J. Powell and T. Jack, *Inorg. Chem.*, **11**, 1039 (1972); P. W. N. M. van Leeuwen and A. P. Praat, *J. Organomet. Chem.*, **21**, 501 (1970); P. W. N. M. van Leeuwen and A. P. Praat, *Recl. Trav. Chim. Pays-Bas*, **89**, 321 (1970).
(7) The program used was LSHAPE (version 3) written by D. A. Couch.
(8) H. S. Gutowsky and C. H. Holm, *J. Chem. Phys.*, **25**, 1228 (1956).
(9) I. O. Sutherland, *Annu. Rep. NMR Spectrosc.*, **4**, 71 (1971).
(10) G. Binsch, *Top. Stereochem.*, **3**, 97 (1968).
(11) S. Glasstone, K. I. Laidler, and H. Eyring, "Theory of Rate Processes", McGraw-Hill, New York, 1941, p 195.
(12) K. G. Denbigh, "Principles of Chemical Equilibrium", Cambridge University Press, London, 1971, p 455.
(13) Small differences in the shapes of the two peaks are attributed to differences in the degrees of rotational freedom associated with the methyl groups of the mono- and bidentate acetate ligands. Similar behavior was noted in the fluorine spectra of the corresponding trifluoroacetato complexes.
(14) The absence of NMR evidence for the intermediate of stereochemistry III in the low-temperature spectra must imply that stereochemistry III is significantly less stable than stereochemistry I for the complex $[Ru(O_2CMe)_2(CO)(PPh_3)_2]$. The same situation prevails for the other complexes discussed in this paper.
(15) D. J. Cole-Hamilton and T. A. Stephenson *J. Chem. Soc., Dalton Trans.*, 754 (1974).
(16) M.J. Church and M. J. Mays, *J. Chem. Soc. A*, 3074 (1968).
(17) H. C. Clark and J. D. Ruddick, *Inorg. Chem.*, **9**, 1226 (1970).
(18) M. B. Hursthouse, unpublished work quoted in ref 5.
(19) The perfluorobenzoate data are not fully consistent with the sequence. However, as noted earlier the perfluorobenzoate spectra displayed extra resonances due to the presence of an additional species which reduces the value of the data obtained from them.
(20) Data for the nitrato complexes come from work in progress. Values of E_a, $\Delta H^{\ddagger}$, $\Delta S^{\ddagger}$, and $\Delta G^{\ddagger}$ are 42 kJ mol^{-1}, 40.5 kJ mol^{-1}, 28 J K^{-1} mol^{-1}, and 35 kJ mol^{-1}, respectively, for $[Ru(NO_3)_2(CO)(PPh_3)_2]$ and 46 kJ mol^{-1}, 44.5 kJ mol^{-1}, 12 J K^{-1} mol^{-1}, and 42 kJ mol^{-1}, respectively, for $[Os(NO_3)_2(CO)(PPh_3)_2]$.